CHALMERS
UNIVERSITY OF TECHNOLOGY

6D Pose Task Trajectory Tracking for a Class of 3D Aerial Manipulator From Differential Flatness

Citation for the original published paper (version of record):
Yu, Y., Lippiello, V. (2019). 6D Pose Task Trajectory Tracking for a Class of 3D Aerial Manipulator From Differential Flatness. IEEE Access, 7: 52257-52265.
http://dx.doi.org/10.1109/ACCESS.2019.2910379

IEEE Access
Multidisciplinary | Rapid Review | Open Access Journal

Received February 12, 2019, accepted March 21, 2019, date of publication April 11, 2019, date of current version April 30, 2019.

Digital Object Identifier 10.1109/ACCESS.2019.2910379

6D Pose Task Trajectory Tracking for a Class of 3D Aerial Manipulator From Differential Flatness

YUSHU YU[1,2] AND VINCENZO LIPPIELLO[3], (Senior Member, IEEE)

[1]School of Mechatronical Engineering, Beijing Institute of Technology, Beijing 10081, China
[2]Department of Mechanics and Maritime Sciences, Chalmers University of Technology, 412 96 Gothenburg, Sweden
[3]Department of Electrical Engineering and Information Technology, University of Naples Federico II, 80138 Naples, Italy

Corresponding author: Vincenzo Lippiello (vincenzo.lippiello@unina.it)

This work was supported in part by the HYFLIERS Project (Horizon 2020) under Grant 779411, and in part by the National Natural Science Foundation of China under Grant 51505014.

ABSTRACT In this paper, the dynamics and control of a novel class of aerial manipulator for the purpose of end effector full pose trajectory tracking are investigated. The 6D pose of the end effector is set as a part of the flat output, from which the conditions that the system has the proposed flat output is obtained. The control law for the end effector tracking purpose is designed. The core part of the controller is an almost global controller in the configuration space of the system. From the transformation between the state space and the output space, the tracking control of the end effector in $SE(3)$ is also achieved. The stability of the controlled system is analyzed. A numerical example is presented to demonstrate the theoretical analysis.

INDEX TERMS Aerial manipulator, task space, tracking control, differential flatness.

I. INTRODUCTION

A. BACKGROUND AND MOTIVATION

Recently, aerial manipulation has attracted great interests in robotics research community [1]. Several groups demonstrated aerial grasping using grippers attached to aerial manipulators [2]–[4]. Lee and Kim, Kim *et al.* show cooperative aerial manipulators grasping with unknown payload in environment with obstacles [5], [6]. Orsag *et al.* demonstrate pick-place and peg-in-hole tasks using quadrotor platform and dual arms attached in the platform [7]. The EU 7-th Framework program funds several projects on aerial manipulators, investigating the motion planning and impedance control with aerial manipulator when interacting with the environment [8]–[10]. A research group in German Aerospace Center presents the potential application of a 7 DOFs anthropomorphic arm attached to a helicopter [11]. Delta-like mechanism [12] and parallel manipulator [13] are also considered in aerial manipulators. Such existing works present a prospective future of research on aerial manipulation. However, compared to ground-based manipulators, the tasks that aerial manipulators can achieve are still in a very preliminary stage. This is due to many factors, such as the end effector of the current aerial manipulators is difficult to achieve 6D pose trajectory tracking.

B. RELATED WORK

It has been shown that the aircraft itself is fully controllable if it is actuated by 1D force and 3D torque. A typical example of such aircraft is quadrotor. In [14], the mechanics and control problem of the quadrotor with a rigidly attached tool effector has been considered. It is found that the 3D force-position control of the quadrotor tool system is possible. However, the end effector needs to be positioned carefully to prevent the unstable internal dynamics induced by the feedback linearization.

In aerial articulated manipulator, the added manipulator joints may compensate for the unstable internal dynamics. By reducing the 3D condition into a 2D condition, the planar quadrotor manipulator presents some good properties [15]–[17]. It was found that the end effector of planar aerial manipulator can achieve trajectory tracking control in $SE(2)$. However, the 3D conditions are different. Most of the previous work on control of 3D aerial articulated manipulator is finished in its configuration space [18]. A regulator for such system is derived and the stability is proven using singular perturbation theory [19]. However the aerial manipulator based on this kind of aircraft is difficult to achieve 6D

The associate editor coordinating the review of this manuscript and approving it for publication was Zheng H. Zhu.

pose trajectory tracking in task space, because of the dynamic coupling between the position and the attitude of such type of aircraft [10]. Yang and Lee propose a back stepping control for position tracking of end effector of quadrotor-based aerial manipulator in [20], where the torque of the aircraft and the joint torque should satisfy dynamic constraints. This makes the joint position difficult to be independently controlled. A method to allocate the joint torque in order to independently control the joint position is also proposed [20], but no proof of controllability is provided.

It is believed that the traditional under-actuated aerial vehicle is not ideal for aerial manipulation, some researchers considered the fully actuated aerial platform-based manipulator. The fully actuated aerial vehicle platform can track the trajectory in $SE(3)$ without any constraints. Franchi et al. propose a fully actuated aerial vehicle where the actuated force and torque is produced by 6 rotors that point to different directions [21]. Other fully actuated aerial platform includes tilting aerial vehicle [22], omni-directional aerial vehicles [23], and aerial vehicles with extra actuators [24]. In summary, the actuators of this class of aerial vehicle can produce 6D independent force and torque. However, the extra actuators also decrease the energy efficiency.

Several researchers also investigated aerial manipulation based on multiple aerial vehicles. It was shown that in 3D space, three quadrotors could lift a rigid body moving in $SE(3)$ [25]. By using a similar principle, Nguyen *et al.* propose a structure for aerial manipulation using multiple quadrotors as rotating thrust generators [26]. These multiple quadrotors connect to the manipulator via spherical joints, the manipulation platform therefore is capable to track a trajectory in $SE(3)$. Six *et al.* propose a flying parallel robot with three quadrotors [27]. This aerial manipulator is composed of three quadrotors which connect to the end effector through light-weight legs. The legs then connect the quadrotor via passive spherical joints and the end effector via passive revolute joints. The multiple aerial vehicle-based manipulator is a possible solution for the 6D pose tracking control of an end effector, though it may also be concluded that it needs a more complex structure.

C. CONTRIBUTIONS

In this paper, the trajectory tracking of the end effector in $SE(3)$ by a single 3D aerial manipulator is investigated. It is well studied that differentially flat systems are input-state feedback linearizable, and are thus controllable [28]. In order to investigate the 6D pose tracking control problem using aerial manipulator, in this paper we set the pose of the end effector as the flat output. The conditions that the 6D pose of the end effector is the flat output are derived and analyzed. It does not need the aircraft base to be fully actuated. In order to deal with the 6D pose trajectory tracking, the flat output is transformed into the state. By designing the state feedback controller, the 6D pose tracking for the end effector is thus achieved. Considering the configuration space of the floating base manipulator is non-Euclidean space, a hybrid controller is designed in order to achieve almost global stability.

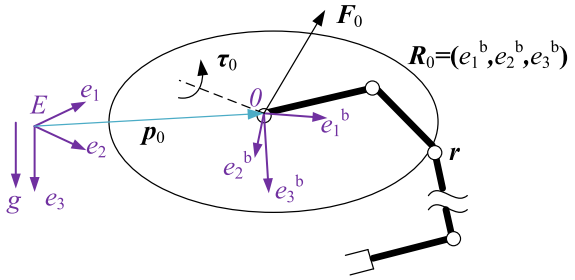

FIGURE 1. Configuration of an aerial manipulator. The first joint locates at the COM of the aircraft base. F_0 and τ_0 are expressed in the floating base fixed frame. The pose of link-i of the manipulator is denoted as $h_i \in SE(3)$. The axis of joint-i expressed in based fixed frame is $z_i \in S^2$. Note the COM of the base is not the COM of the entire system.

Overall, the main contribution of this paper can be summarized as follows. 1) To the authors' best of knowledge, this paper proposes a new class of aerial manipulator for 6D pose task trajectory tracking for the first time. Unlike the fully actuated aerial platform which usually needs three linear actuation force, the proposed aerial platform needs only two actuation force. 2) The fact that the task space of the proposed aerial manipulator is 6D is proven from differential flatness. 3) For the 6D pose task trajectory tracking purpose, a control framework for the proposed class of aerial manipulator is designed and analyzed.

This paper is organized as follows: The dynamics and the analysis of the differential flatness of the system are presented in Section II. In Section III, the controller for full pose tracking in task space is designed and analyzed. In Section IV, a numerical simulation for the proposed class of aerial manipulator is demonstrated.

II. PROBLEM FORMULATION

A. SYSTEM MODELING OF AERIAL MANIPULATOR

1) CONFIGURATION, VELOCITY AND DYNAMICS

As shown in Fig. 1, for an aerial manipulator system composed with a floating base and a n-joint manipulator, the configuration of the system is denoted by $q = (h_0, r) \in SE(3) \times \mathbb{R}^n$, where $h_0 = \begin{bmatrix} R_0 & p_0 \\ 0 & 1 \end{bmatrix}$ is the pose of the floating base, $r \in \mathbb{R}^n$ is the joint position. The system's velocity is given by $\zeta = (V, \dot{r}) \in \mathbb{R}^6 \times \mathbb{R}^n$, where $V = (v_0, \omega_0)$ is the *body* velocity of the aircraft base. The dynamic equation of the system can thus be expressed in these notations as [1],

$$M_t(r)\dot{\zeta} + C_t(r, \zeta)\zeta + G_t(r, R_0) = u \tag{1}$$

where $M_t(r)$, $C_t(r, \zeta)$, $G_t(r, R)$ are the mass matrix, Coriolis matrix, and gravity vector respectively, and $u = (F_0, \tau_0, \tau_r)$ is the input of the system. The mass matrix $M_t(r)$ is symmetric positive definite.

2) PASSIVE DECOMPOSITION OF DYNAMICS

The system equation (1) reveals the properties of underactuation and coupling. In order to investigate the planning and

control solution of this system, we split the tangent space of (1) using the passive decomposition method presented in [20] as

$$\zeta = \begin{bmatrix} \Delta_\perp & \Delta_\top \end{bmatrix} \begin{bmatrix} {}^b\dot{p} \\ \mu \end{bmatrix} := \underbrace{\begin{bmatrix} I_3 & S_E(r) \\ 0 & I_{n+3} \end{bmatrix}}_{S(r)} \eta \tag{2}$$

where $\mu = (\omega_0, \dot{r}) \in \mathbb{R}^{3+n}$, ${}^b\dot{p}$ is the linear velocity of the center of mass (COM) of the entire system expressed in floating base fixed frame, I represents the identity matrix, $S_E(r) \in \mathbb{R}^{3\times(n+3)}$, $S(r) \in \mathbb{R}^{(n+6)\times(n+6)}$. Transforming the *body* linear velocity ${}^b\dot{p}$ to *spatial* linear velocity $\dot{p}$, we can thus obtain the decoupled equation of motion (EOM) as [20],

$$\begin{aligned} &\text{locked system} \quad \begin{cases} \dot{p} = v \\ \dot{v} = \frac{1}{m} R_0 F_0 + g e_3 \end{cases} \\ &\text{shape system} \quad \begin{cases} \dot{\sigma} = \sigma \hat{\mu} \\ M(r)\dot{\mu} + C(r,\mu)\mu = S_E^T F_0 + \begin{bmatrix} \tau_0 \\ \tau_r \end{bmatrix} \triangleq \tau_E \end{cases} \end{aligned} \tag{3}$$

where $\sigma = (R_0, r) \in SO(3) \times \mathbb{R}^n$, m is the total mass, g is the acceleration due to gravity, e_i denotes the canonical basis vector in $\mathbb{R}^3$, e.g., $e_3 = (0, 0, 1)^T$, the operation $\sigma\hat{\mu} = \left(R_0^T \hat{\omega}_0, \dot{r}\right)$ represents the tangent map induced by the left translation on $SO(3) \times \mathbb{R}^n$. This decomposition partitions the whole system into two subsystems: the *locked system* describing the translational motion of the COM defined on $\mathbb{R}^3$, and the *shape system* describing the rotational motion of the whole system on $SO(3) \times \mathbb{R}^n$. Note that in (3), p and v are the position and velocity of COM of the entire system expressed in *Earth* frame.

B. FLAT OUTPUT DEFINITION

In order to let the end effector be able to track the trajectory in $SE(3)$, and also to let the joint angles track the reference trajectories, a natural selection of the flat output of the system is (h_t, r), where $h_t = \begin{bmatrix} R_t & p_t \\ 0 & 1 \end{bmatrix} \in SE(3)$ is the task space coordinate which is the pose of the end effector. However, this choice needs the aircraft to be fully actuated. In this paper, we consider the following flat output $y_1 = (h_t, (r_2, r_3, \ldots, r_n))^T$.

Problem 1: Given the system dynamics (1) and the reference flat output $y_{1,d} : t \mapsto y_1(t) \in SE(3) \times \mathbb{R}^{n-1}$, design control u such that $y_1 \to y_{1,d}$ along the trajectory defined by (1).

Lemma 1: Given a constant $z \in S^2$, define the following sets, $\Omega_R = \{R \in SO(3) | Rz \neq -z\}$, $\tilde{S}^2 = S^2/(-z)$, and $\Omega_{R_p} = \{R \in SO(3) | R = \exp(\theta\hat{z}), \theta \in \mathbb{R}\}$. Then there exists a mapping $f_z : \Omega_R \mapsto \tilde{S}^2 \times \Omega_{R_p}$ which is a diffeomorphism.

Proof: In the proof, first we will define smooth functions: f_z and its inverse f_z^{-1}, then we will show f_z is bijection.

(i) For all $R \in \Omega_R$, one can define

$$z_b = Rz \tag{4}$$

And $\forall z_b \neq -z$ one can define a unique rotation matrix

$$R_l = \begin{cases} \exp(\vartheta\hat{q}), z_b \neq z \\ I, z_b = z \end{cases} := f_{R_l}(R, z) \tag{5}$$

where the $\vartheta \in [0, \pi]$ is the eigen-angle of R_l, it is defined as the angle from z to z_b

$$\vartheta = \cos^{-1}(1 - \frac{1}{2}\|z - z_b\|^2)$$

and the eigen-axis $q \in S^2$ of R_l is defined by

$$q = \frac{z \times z_b}{\|z \times z_b\|}, \quad z \neq z_b$$

Expanding the expression of $\exp(\vartheta\hat{q})$ we have,

$$f_{R_l}(R, z) = \begin{cases} I + (z \times Rz)\hat{} \\ \quad + \frac{1}{1 + z^T Rz} \left((z \times Rz)\hat{}\right)^2, \quad z_b \neq z. \\ I, z_b = z \end{cases} \tag{6}$$

Then we define

$$R_p = R_l^T R. \tag{7}$$

It is seen from (5)

$$R_l z = z_b = Rz. \tag{8}$$

Then from (7) and (8) we have

$$R_p z = z. \tag{9}$$

Therefore the eigen-axis of R_p is z, which means $R_p \in \Omega_{R_p}$. From (4)–(7) we have defined the smooth mapping $f_z : \Omega_R \ni R \mapsto (z_b, R_p) \in \tilde{S}^2 \times \Omega_{R_p}$.

(ii) For any element $(z_b, R_p) \in \tilde{S}^2 \times \Omega_{R_p}$, one can calculate $R_l \in SO(3)$ from z_b according to (5), then calculate $R = R_l R_p$ which is an element in Ω_R. The smooth mapping $f_z^{-1} : (\tilde{S}^2 \times \Omega_{R_p}) \ni (z_b, R_p) \mapsto R \in \Omega_R$ is therefore obtained.

(iii) Then we will show f_z is bijection.

Consider $R_1, R_2 \in SO(3), R_1 \neq R_2$. If $R_1 z = R_2 z$, calculate $R_{1,l}$ and $R_{2,l}$ from R_1 and R_2 according to (5), we have $R_{1,p} = R_{1,l}^T R_1, R_{2,p} = R_{2,l}^T R_2$, it is seen $R_{1,l} = R_{2,l}$, but $R_{1,p} \neq R_{2,p}$ because $R_1 \neq R_2$, therefore $f_z(R_1) \neq f_z(R_2)$. Else if $R_1 z \neq R_2 z$, it is obvious that $f_z(R_1) \neq f_z(R_2)$. Therefore f_z is one-to-one.

During the previous proof, it has shown that f_z is onto, since $\forall (z_b, R_p) \in (\tilde{S}^2 \times \Omega_{R_p}), f_z^{-1}(z_b, R_p) \in \Omega_R$. Therefore we can conclude that f_z is bijection. This completes the proof. ■

Remark 1: The physical meaning of Lemma 1 is that the attitude of a rigid body can be represented as the attitude of a body-fixed axis, and a rotational angle around the axis, as shown in Fig. 2. Considering an attitude trajectory of the rigid body $R(t) : \mathbb{R} \geq 0 \mapsto \Omega_R$. From Lemma 1, one can also obtain the corresponding trajectory $R_l(t), R_p(t) : \mathbb{R} \geq 0 \mapsto (\Omega_{R_l} \times \Omega_{R_p})$, where $\Omega_{R_l} \subset SO(3)$ denotes the set of R_l defined in (5). The smooth mapping f_z also induces the tangent mapping $f_{z,*R} : \dot{R} \in T_R\Omega_R \mapsto T_{f_z(R)}(\tilde{S}^2 \times \Omega_{R_p}) \ni (\dot{z}_b, \dot{R}_p)$, where $\dot{z}_b = \dot{R}z, \dot{R}_p = R_p\hat{z}\dot{\theta}$, therefore we can express $\dot{\theta}$ as

$$\dot{\theta} = \langle (R_p^T \dot{R}_p)^\vee, z \rangle \quad := f_{\dot{\theta}}(\dot{R}, R) \tag{10}$$

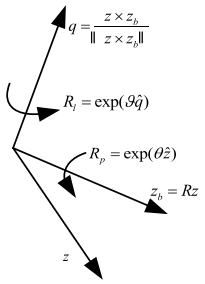

FIGURE 2. The attitude of a rigid body can be represented by the attitude of a body-fixed axis, and the rotational motion around the body-fixed axis.

where $\langle ., . \rangle$ represents the inner product of two vectors.

Remark 2: In Lemma 1, Ω_R is a subset of $SO(3)$. It should be noticed that for $R \in \Omega_s = \{R \in SO(3) | Rz = -z\}$, we cannot define R_p using Lemma 1, as R_l calculated through (5) has infinite possibilities. This singularity will not be considered in this paper.

Proposition 1: Consider the aerial manipulation system with configuration shown in Fig. 1 and dynamics (1), suppose $R_0\, z_1 \neq -z_1$. Define variable $y_2 = (p, R_{0,l}, r_1^a, r_2, r_3, \ldots, r_n)$, where $R_{0,l} = f_{R_l}(R_0, z_1)$, $r_1^a = r_1 + \phi$, and ϕ is determined from $\exp(\phi \hat{z}_1) = R_{0,l}^T R_0$. Then $\Omega_{y_1} = \{y_1\}$ is diffeomorphic to $\Omega_{y_2} = \{y_2\}$.

Proof: It is seen that Ω_{y_1} and Ω_{y_2} are both $n + 5$ dimensional. In order to prove this proposition, first we will show that $y_2 \mapsto h_t$ is smooth function, second we will show that $y_1 \mapsto p$ and $y_1 \mapsto R_{0,l}$ are also smooth functions.

First we show the transformation from y_2 to y_1. The attitude of the first link of the manipulator is given by

$$R_1 = R_{0,l} \exp(r_1^a \hat{z}_1). \tag{11}$$

The attitude of the remaining links of the manipulator is determined as

$$R_i = R_1 \prod_{j=2}^{i} \exp(r_j \hat{z}_j), \quad i = 2, \ldots, n. \tag{12}$$

Because joint-1 locates in the COM of the base, the attitude of the base has no effect on p, the position of the end effector can thus be expressed as

$$p_t = f_{p_t}(p, R_1, R_2, \ldots, R_n). \tag{13}$$

Combining (11), (12), and (13), we conclude $y_2 \mapsto h_t$ is a smooth function.

Then, we show the transformation from y_1 to y_2. Given y_1, it is easy to solve h_1. Therefore, p is expressed as $p = f_p(h_1, r_2, \ldots, r_n)$. Furthermore, from Lemma 1 we have $R_{0,l} = R_{1,l} = f_{R_l}(R_1, z_1)$, and $r_1^a = \langle (\exp^{-1}(R_{1,p}))^\vee, z_1 \rangle$. The smooth map $y_1 \mapsto y_2$ is thus achieved. Therefore the diffeomorphism between Ω_{y_1} and Ω_{y_2} is proven. ■

Theorem 1: Consider the system dynamics (1), suppose $R_0\, z_1 \neq -z_1$, and $(\ddot{p} - g e_3) \times (R_0\, z_1) \neq 0$. If $\{(\tau_0, \tau_r)\} = \mathbb{R}^{3+n}$ and $\{F_0\} = \text{span}(z_1, z_1^\perp)$, where $z_1^\perp \in S^2$ is s.t. $z_1^\perp \perp z_1$, span$(*)$ represents the space spanned by each column of $*$, then y_1 is the flat output of the system (1).

Proof: First we prove that y_2 is the flat output of the system.

For brevity, we write $F_d = m\ddot{p}$, it is seen

$$F_d = R_0 F_0 + mge_3 \tag{14}$$

where R_0 can be expressed using Lemma 1 as

$$R_0 = R_{0,l} \exp(\phi \hat{z}_1).$$

Therefore

$$\exp(\phi \hat{z}_1) F_0 = {R_{0,l}}^T (F_d - mge_3). \tag{15}$$

If $F_0 \in \text{span}(z_1, z_1^\perp)$, assuming ϕ is unbounded, then from the flat output $(R_{0,l}, \ddot{p})$ we can always solve input F_0 along z_1 and $z_1^\perp$ as

$$\begin{aligned} \langle F_0, z_1 \rangle &= [(F_d - mge_3)^T R_{0,l} z_1] \\ \langle F_0, z_1^\perp \rangle &= \sqrt{\| R_{0,l}^T (F_d - mge_3) \|^2 - \| \langle F_0, z_1 \rangle \|^2} \end{aligned} \tag{16}$$

We define $R_z = (z_1, z_1^\perp \times z_1, z_1^\perp)$, because $z_1 = R_z e_1$ we can rewrite the force allocation (15) as follows,

$$R_z \exp(\phi \hat{e}_1) R_z^T R_z \begin{bmatrix} F_0^T z_1 \\ 0 \\ F_0^T z_1^\perp \end{bmatrix} = {R_{0,l}}^T (F_d - mge_3) \tag{17}$$

where $\exp(\phi \hat{e}_1) = (e_1, e_{2\phi}, e_{3\phi})$ can be solved as,

$$e_{3\phi} = \frac{R_z^T R_{0,l}^T (F_d - mge_3) - (F_0^T z_1) e_1}{F_0^T z_1^\perp}, \quad F_0^T z_1^\perp \neq 0$$

and $e_{2\phi} = e_{3\phi} \times e_1$. Then, the attitude of the aircraft base can be calculated as

$$R_0 = R_{0,l} R_z \exp(\phi \hat{e}_1) R_z^T. \tag{18}$$

The joint angle of the first joint is then solved as

$$r_1 = r_1^a - \phi. \tag{19}$$

By now, we have shown that R_0 and r_1 are algebraic functions of $\ddot{p}$ and $R_{0,l}$. Since $\hat{\omega}_0 = R_0^T \dot{R}_0$, it is not difficult to derive ω_0 and $\dot{r}$ from $\ddot{p}$, $R_{0,l}$, $\dddot{p}$, $\dot{R}_{0,l}$, and $(\dot{r}_2, \ldots, \dot{r}_n)$. And since $\{(\tau_0, \tau_r)\} = \mathbb{R}^{3+n}$, the shape system is fully actuated, therefore (τ_0, τ_r) can also be derived from $\ddot{p}$, $R_{0,l}$, $\dddot{p}$, $\dot{R}_{0,l}$, $\ddddot{p}$, $\ddot{R}_{0,l}$, $(\dot{r}_2, \ldots, \dot{r}_n)$, and $(\ddot{r}_2, \ldots, \ddot{r}_n)$. For brevity the detailed derivation is not presented here. The proof that y_2 is the flat output is thus finished.

Since Ω_{y_1} and Ω_{y_2} are diffeomorphic, once y_2 is the flat output, y_1 is also the flat output. ■

Remark 3: $\{F_0\} = \text{span}(z_1, z_1^\perp)$ is possible to be realized in physical systems. The approach includes adding tilting actuators, or extra actuators on the aircraft base. As seen in Theorem 1, the force acting on the aircraft body is restricted to 2D space. Therefore the aircraft platform is not a fully actuated aerial vehicle which usually needs three independent forces, thus is more efficient than the fully actuated aerial vehicle.

Remark 4: Another approach to contain $h_t \in SE(3)$ in flat output space is to let $\{\tau_1\} = \mathbb{R}^2$ [29]. The proof can be correspondingly derived. However, it is seen that this condition is not easy to be realized in physical systems. Therefore, this paper focuses on the aerial manipulator with conditions shown in Theorem 1.

Remark 5: Both y_1 and y_2 contain the joint position $r_2, \ldots, r_n$. It is seen under the conditions in Theorem 1, $r_2, \ldots, r_n$ is redundant for tracking h_t. However, $r_2, \ldots, r_n$ is useful for increasing the flexibility of the manipulation, e.g., it can increase the workspace of the end effector.

III. GLOBAL CONTROL DESIGN AND STABILITY ANALYSIS

A. CONTROL STRATEGY

Theorem 1 gives conditions for u, in order to solve Problem 1, we need to design the control law for u. To let $h_t \to h_{t,d}$, one needs to express the system dynamics with respect to p_t and R_t. It is seen that $\dot{p}_t$ and $\dot{R}_t$ are highly coupled with the rotational part of the body dynamics, as well as the joint position dynamics. The system dynamics with respect to h_t thus is quite complex. To avoid the complex expressions, the control strategy is to ensure $y_2 \to y_{2,d}$, then use the diffeomorphism between Ω_{y_1} and Ω_{y_2} to let $y_1 \to y_{1,d}$. The overall control strategy is shown in Fig. 3.

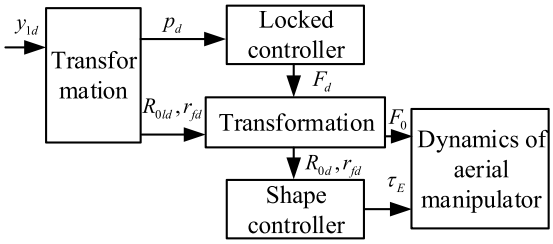

FIGURE 3. Overall control strategy.

In order to achieve $y_2 \to y_{2,d}$, a controller with a cascade structure is designed. Given the smooth trajectory $y_{2,d}$, $R_{0,d}$ can be calculated from the flatness of the system. The inner loop control is to guarantee $R_0 \to R_{0,d}$ and $r_f \to r_{f,d}$, where $r_f = (r_1^a, r_2, \ldots, r_n)^T$, the outer loop control is to guarantee $p \to p_d$. In this way, the controller is possible to stabilize the entire $12 + 2\,n$ dimensional state.

First we write the dynamics of the shape system with respect to r_f. Differentiate (19) and combine (10), we can obtain the expression of $\dot{r}_1$ as

$$\dot{r}_1 = \dot{r}_1^a - f_{\dot{\theta}}(\dot{R}_0, R_0). \tag{20}$$

Substituting (19) and (20) into (3), we can write the dynamics of the shape system with respect to r_f as,

$$M(r)\dot{\mu}_f + C_f(r_f, R_0, \mu_f)\mu_f = \tau_E \tag{21}$$

where $\mu_f = (\omega_0, \dot{r}_f) \in \mathbb{R}^{3+n}$ represents the velocity, and the Coriolis part becomes:

$$C_f(r_f, R_0, \mu_f)\mu_f = C(r, \mu)\mu - M(r)\begin{bmatrix} 0 \\ f_{\dot{\theta}}(\dot{R}_0, R_0) \\ 0 \end{bmatrix}.$$

B. DEFINITION OF THE TRACKING ERROR FOR SHAPE SYSTEM

The configuration space of the shape system is $SO(3) \times \mathbb{R}^n$ which is a non-Euclidean space [30]. In order to achieve almost global control at $SO(3) \times \mathbb{R}^n$, considering the topological structure of the manifold $SO(3)$, we use exponential coordinate to represent the attitude, and with the help of hybrid system theory, we construct the hybrid formulation of the dynamics. The reason why to use such a structure is that the expression physically reveals the geometric properties of the error on $SO(3)$. The property can be seen in [31, Lemma 1].

We rewrite the equation of rotational motion of a rigid body with inertia tensor $I_r \in \mathbb{R}^{3\times3}$ in a hybrid form as,

$$\mathcal{H}: \begin{cases} \begin{cases} \dot{\xi} = J_a(\xi)\omega \\ \dot{\omega} = I_r^{-1}\left(\tau - \hat{\omega} I_r \omega\right) \end{cases} & , \quad (\xi, \omega) \in S_C \\ \begin{cases} \xi^+ = \xi^- - 2\pi \frac{\xi^-}{\|\xi^-\|} \\ \omega^+ = \omega^- \end{cases} & , \quad (\xi, \omega) \in S_D \end{cases}. \tag{22}$$

with flow set S_C and jump set S_D,

$$\begin{aligned} S_D &= \left\{(\xi, \omega) : ||\xi|| = r, \left\langle \dot{\xi}, \xi \right\rangle > 0\right\} \\ S_C &= \{(\xi, \omega) : (\xi, \omega) \notin S_D\} \end{aligned} \tag{23}$$

where ξ is the exponential coordinates of R, and is restricted in a ball $B_a = \{\xi \in \mathbb{R}^3 : \|\xi\| \le r, \pi \le a < 2\pi\}$.

Based on (22), the tracking error EOM of the shape system with respect to r_f can be expressed as,

$$\begin{cases} \begin{cases} \dot{\gamma}_e = J(\gamma_e)\mu_{f,e} \\ \dot{\mu}_{f,e} = \varphi(\tau_E, \mu_{f,e}, \gamma_e, R_{0,d}, \dot{R}_{0,d}, \ddot{R}_{0,d}) \end{cases} & , \left(\gamma_e, \mu_{f,e}\right) \in S_C \\ \begin{cases} \gamma_e^+ = (\xi_e^- - \frac{2\pi}{a}\xi_e^-, r_f^-) \\ \mu_{f,e}^+ = (\mu_{f,e}^-, \dot{r}_{f,e}^-) \end{cases} & , \quad \left(\gamma_e, \mu_{fe}\right) \in S_D \end{cases} \tag{24}$$

where ξ_e is the attitude tracking error calculated from $\exp(\xi_e) = R_{0,d}^T R_0 := R_{0,e}$, $\gamma_e = (\xi_e, r_{f,e})$ is the representation of configuration error, $\mu_{fe} = (\omega_e, \dot{r}_{f,e})$ is the velocity tracking error, $J(\gamma_e) = \begin{bmatrix} J_\alpha(\xi_e) & 0 \\ 0 & I_n \end{bmatrix}$.

Considering in real-time systems, there are always noises, which may make the hybrid system chatter frequently. Therefore the definition of the set of ξ_e is modified to,

$$\Omega_{\xi_e} = \left\{\xi_e \in \mathbb{R}^3 : \|\xi_e\| \le \pi + \delta\right\} := B_{\pi+\delta} \tag{25}$$

where δ is a small positive constant to prevent frequent jump due to the noises. S_D for ξ_e is then revised to,

$$S_D = \{\xi_e \in B_{\pi+\delta} : \|\xi_e\| = \pi + \delta, \langle \omega_e, \xi_e \rangle > 0\}. \tag{26}$$

C. GLOBAL TRACKING CONTROL OF SHAPE SYSTEM

Assumption 1: For every $j = 1, \ldots, n$, the joint velocity $\dot{r}_j$ is bounded, and the Jacobian matrix $J_j(r)$ expressed in aircraft base fixed frame is smooth function with respect to r.

Lemma 2: The eigenvalue of $\dot{M}(r)$ is bounded under Assumption 1.

Proof: The mass matrix $M_t(r)$ can be expressed as $M_t(r) = (m_0 J_{v0}^T J_{v0} + J_{\omega 0}^T I_{r,0} J_{\omega 0}) + \sum_{j=1}^{n} (m_j J_{vj}^T J_{vj} + J_{\omega j}^T {}^0R_j I_{r,j} {}^0R_j^T J_{\omega j})$, where J_{vj} and $J_{\omega j}$ represent the translational and rotational Jacobian matrix of link-j. If J_{vj} and $J_{\omega j}$ are smooth function of r and $\dot{r}$ is bounded, then $\dot{M}_{t,ij} = \frac{\partial M_{ij}(r)}{\partial r}\dot{r}$ is also bounded, where $M_{t,ij}$ is the (i, j) element of $M_t(r)$. Similarly, we can also obtain that each element of $\dot{S}_E(r)$ is bounded. This implies that $\|\dot{M}\|_1$ is bounded. From the equivalence of 1-norm and 2-norm, we can conclude the boundedness of $\|\dot{M}\|_2$, which implies that $\lambda(\dot{M})$ is bounded. ∎

We denote $\lambda_m(.)$ and $\lambda_M(.)$ the min and max eigenvalue function of a matrix. By defining the tracking error dynamics, the global tracking control of shape system is the same to the stabilization control of (24) at $(\gamma_e, \mu_{f,e}) = (0, 0)$. For this purpose, we design the following control law,

$$\tau_E = -k_\gamma \gamma_e - k_\mu \mu_{f,e} + C_f \mu_f - M \begin{bmatrix} \hat{\omega}_0 \exp(-\hat{\xi}_e)\omega_{0,d} - \exp(-\hat{\xi}_e)\dot{\omega}_{0,d} \\ -\ddot{r}_{f,d} \end{bmatrix} \tag{27}$$

where k_γ and k_μ are positive constants s.t.

$$k_\mu > \frac{1}{2}\lambda_M(\dot{M}). \tag{28}$$

Theorem 2: Consider the tracking error system expressed by (24), the control input τ_E is given by (27), suppose the positive definite constants k_γ, k_μ s.t. (28). Then the equilibrium point $(\gamma_e, \mu_{f,e}) = (0, 0)$ is the only equilibrium point, and it is exponentially stable (ES) on $(B_{\pi+\delta} \times \mathbb{R}^n) \times \mathbb{R}^{3+n}$.

Proof: Substituting the control law (27) into (24) obtains the following closed loop equation for the shape system,

$$\begin{aligned} \dot{\gamma}_e &= J(\gamma_e)\mu_{f,e} \\ M\dot{\mu}_{f,e} &= -k_\gamma \gamma_e - k_\mu \mu_{f,e}. \end{aligned} \tag{29}$$

Since the attitude error is defined in a compact set, $J(\gamma_e)$ is always non-singular, therefore $J(\gamma_e)\mu_{f,e} = 0, -k_\gamma \gamma_e - k_\mu \mu_{f,e} = 0$ has only one solution $(\gamma_e, \mu_{f,e}) = (0, 0)$.

Consider the following Lyapunov candidate with a positive constant c,

$$V = \frac{1}{2}\langle \mu_{f,e}, M\mu_{f,e}\rangle + \frac{1}{2}k_\gamma \langle \gamma_e, \gamma_e\rangle + c\langle \gamma_e, \mu_{f,e}\rangle. \tag{30}$$

In order to investigate the positive definite property of V, construct the positive definite matrix candidate $W_1 = \begin{bmatrix} \frac{1}{2}k_\gamma & \frac{c}{2} \\ \frac{c}{2} & \frac{1}{2}\lambda_M(M) \end{bmatrix}$ and $W_2 = \begin{bmatrix} \frac{1}{2}k_\gamma & -\frac{c}{2} \\ -\frac{c}{2} & \frac{1}{2}\lambda_m(M) \end{bmatrix}$, The boundedness of V can be expressed as,

$$e_s^T W_2 e_s \le V \le e_s^T W_1 e_s \tag{31}$$

where $e_s = \left(\|\gamma_e\|, \|\mu_{f,e}\|\right)^T$.

The stability analysis is finished in two steps. First, we differentiate (30) to investigate $\dot{V}$ in S_C. Because $\langle \dot{\xi}, \xi\rangle = \langle \omega, \xi\rangle$, we have,

$$\begin{aligned} \dot{V} &= \langle \mu_{f,e}, M\dot{\mu}_{f,e}\rangle + \langle k_\gamma \gamma_e, \dot{\gamma}_e\rangle + \langle c\dot{\gamma}_e, \mu_{f,e}\rangle + \\ &\quad \langle c\gamma_e, \dot{\mu}_{f,e}\rangle + \frac{1}{2}\langle \mu_{f,e}, \dot{M}\mu_{f,e}\rangle \\ &= -\left(\langle c\gamma_e, M^{-1}k_\gamma \gamma_e\rangle + \langle c\gamma_e, M^{-1}k_\mu \mu_{f,e}\rangle\right) + \\ &\quad -\left(\langle \mu_{f,e}, k_\mu \mu_{f,e}\rangle - \langle cJ(\gamma_e)\mu_{fe}, \mu_{f,e}\rangle - \frac{1}{2}\langle \mu_{f,e}, \dot{M}\mu_{f,e}\rangle\right). \end{aligned} \tag{32}$$

We also construct a matrix W_3,

$$W_3 = \begin{bmatrix} \frac{ck_\gamma}{\lambda_M(M)} & -\frac{ck_\mu}{2\lambda_m(M)} \\ -\frac{ck_\mu}{2\lambda_m(M)} & k_\mu - c\max\limits_{\xi\in B}\|J(\gamma_e)\|_2 - \frac{1}{2}\lambda_M(\dot{M}) \end{bmatrix}.$$

Then we have

$$\dot{V} \le -e_1^T W_3 e_1. \tag{33}$$

If c satisfies

$$c < \min\left\{\sqrt{k_\gamma \lambda_m(M)}, \frac{\lambda_m^2(M)k_\gamma\left(k_\mu - \frac{1}{2}\lambda_M(\dot{M})\right)}{\lambda_m^2(M)k_\gamma \max\limits_{\xi\in B}\|J(\gamma_e)\|_2 + \frac{1}{4}\lambda_M(M)k_\mu^2}\right\}, \tag{34}$$

and let k_γ, k_μ s.t. (28), then W_1, W_2, W_3 are all positive definite matrix. Then V and $\dot{V}$ satisfy

$$V > 0, \quad \dot{V} < 0. \tag{35}$$

In order to show the exponential stability, define $\alpha = \frac{\lambda_m(W_3)}{\lambda_M(W_1)}$, it can be found that $\dot{V}$ during the flow map further satisfies

$$\dot{V} \le -\alpha V. \tag{36}$$

The second step is to investigate the flow of V during the jump map. From the definition of S_D in (24) we have,

$$\begin{aligned} V^+ - V^- &= \frac{1}{2}k_\gamma \langle \gamma_e^+, \gamma_e^+\rangle - \frac{1}{2}k_\gamma \langle \gamma_e^-, \gamma_e^-\rangle \\ &\quad + c\langle \gamma_e^+, \mu_{f,e}^+\rangle - c\langle \gamma_e^-, \mu_{f,e}^-\rangle. \end{aligned} \tag{37}$$

Considering the jump conditions, it is concluded

$$V^+ < V^- \tag{38}$$

is always found for any jump of $(\gamma_e, \mu_{f,e})$.

Combining (35), (36), (38), from the stability of hybrid systems [32], the ES of the system (22) on $(B_{\pi+\delta} \times \mathbb{R}^n) \times \mathbb{R}^{3+n}$ is achieved. ■

Remark 6: Considering the properties of exponential map, the ES at $(\gamma_e, \mu_{f,e}) = (0, 0)$ is the same as the global exponential stability (GES) of $(R_{0,e}, r_{f,e}, \mu_{f,e}) = (I, 0, 0)$ on $(SO(3) \times \mathbb{R}^n) \times \mathbb{R}^{3+n}$.

D. TRACKING CONTROL OF END EFFECTOR

In order to let $y_2 \to y_{2,d}$, we design the locked controller to ensure $p \to p_d$. For this purpose, design the control law for F_d

$$F_d = m(-k_T e_l + \ddot{p}_d), \tag{39}$$

where $e_l = [p_e^T, \dot{p}_e^T]^T$, $p_e = p - p_d$, and $k_T = \left(k_p, k_v\right) \in \mathbb{R}^{3\times 6}$ is composed of positive definite diagonal matrix k_p and k_v.

Theorem 3: Consider the system dynamics (1), given smooth reference trajectory $y_{2,d} = (p_d, R_{0,l,d}, r_{f,d})$, the control law is designed from (27) and (39), $R_{0,d}$ is transformed from $(R_{0,l,d}, F_d)$ using (18), F_d and $R_{0,d}$ satisfies $R_{0,d}z_1 \neq -z_1$ and $(F_d - mge_3) \times (R_{0,d}z_1) \neq 0$. Then $y_2 \to y_{2,d}$ asymptotically.

Proof: By considering the tracking error R_{0e}, the position tracking error dynamics of the COM can be expressed as,

$$\dot{e}_l = \begin{bmatrix} 0 & I \\ 0 & 0 \end{bmatrix} e_l + \begin{bmatrix} 0 \\ I \end{bmatrix} \left(\frac{F_d}{m} - \ddot{p}_d\right) + \begin{bmatrix} 0 \\ \Delta_p \end{bmatrix}. \tag{40}$$

Once $R_0 \to R_{0,d}$ exponentially, the boundedness of Δ_p can be proven [31]. Then system (40) is stable at $e_l = 0$. From the stability of the system in cascade, it is shown $p \to p_d, R_0 \to R_{0,d}, r_f \to r_{f,d}$ asymptotically for the entire system. ■

Remark 7: Because Ω_{y_1} is diffeomorphic to Ω_{y_2}. From the fact that $y_2 \to y_{2,d}$ asymptotically, we can also conclude that $y_1 \to y_{1,d}$ asymptotically. Problem 1 is therefore solved. This controller is stable except at $(F_d - mge_3) \times (R_{0,d}z_1) = 0$, or $R_0\, z_1 = -z_1$.

Remark 8: Theorem 3 does not consider the external perturbations. However, it can be proven that for bounded regular perturbations, the tracking error of the closed loop system can be kept in an invariant set containing origin [33]. Moreover, there are some methodologies which enable us to add adaptive control law on (27) and (39) to force the tracking error to converge to origin at the presence of bounded perturbations [31], [34]. The details are not discussed here due to the fact that it is not the focus of this paper.

IV. NUMERICAL EXAMPLE

In the simulation, an aerial manipulator system with a two-joint manipulator is adopted as an example. The inertial tensors of the system are

$$I_{r,0} = \text{diag}(0.0294853, 0.0636259, 0.0809362)$$
$$I_{r,1} = \text{diag}(0.00001992, 0.00022247, 0.0002224)$$
$$I_{r,2} = \text{diag}(0.00001868, 0.00040523, 0.00041661)$$

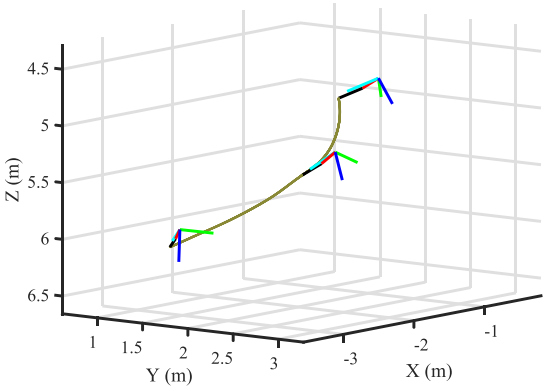

FIGURE 4. The 3D snapshots from 5 s to 6 s. The cyan, green, and blue color line represent R_0e_1, R_0e_2, and R_0e_3 respectively. The red and black line represent link-1 and link-2 of the manipulator.

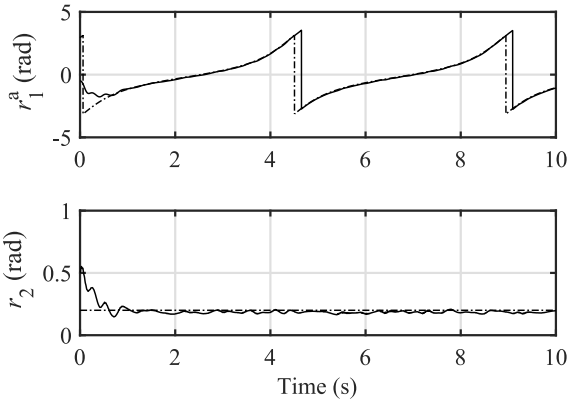

FIGURE 5. Tracking profile of r_f. Dot-dashed line represents $r_{f,d}$.

with unit of kg · m^3. The force F_0 is on the plane span$(e_2, -e_3)$. The joint axes are all set to e_2. In the simulation, the system's initial configuration is given by

$$q = \left(\begin{bmatrix} & & 1 \\ I & & 0 \\ & & 0 \\ 0 & & 1 \end{bmatrix}, [-0.5, 0.5] \right).$$

The desired pose of the end effector is given by $p_{t,d} = (2\cos(\sqrt{2}t) - 2, 2\sin(\sqrt{2}t), t)$. which is a screw-like trajectory. The desired attitude of the end effector is $R_{t,d} = \exp\left((\sqrt{2}t + \pi)\hat{a}\right)$, where $a = (0, 0.5, 1)^T / \frac{\sqrt{5}}{2}$. The desired position of the second joint is $r_{2,d} = 0.2$ rad.

Equation (1) is adopted as the plant EOM in the simulation. In order to test the robustness of the controller, the following factors are added in the simulation.

1) 20% uncertainties are added to the inertial parameters used in the controller.

2) Random external disturbances with maximum absolute value of $d_m = (2, 2, 2, 0.2, 0.2, 0.2, 0.1, 0.1)^T$ is added on F_0 and τ_0, with units in SI.

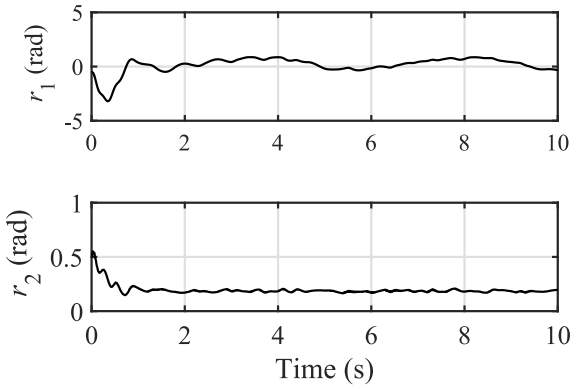

FIGURE 6. Joint position $r(t)$.

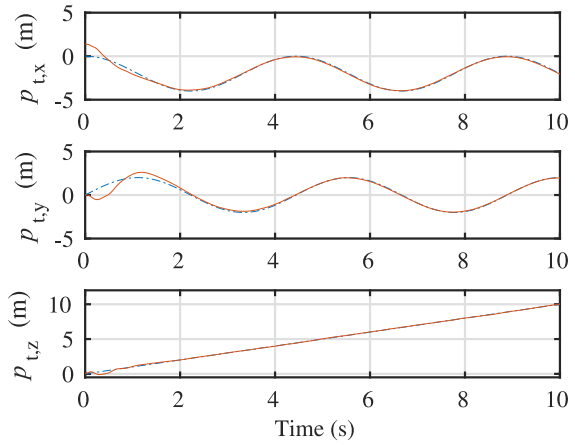

FIGURE 7. Tracking profile of the end effector position.

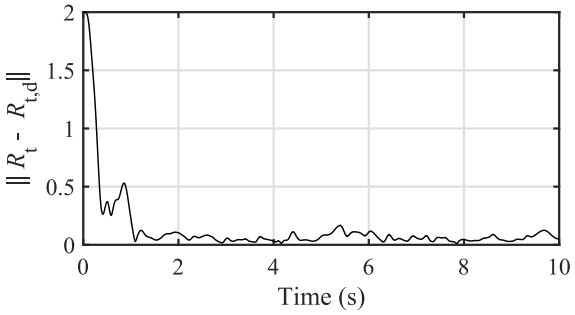

FIGURE 8. The attitude tracking error of the end effector.

3) The following first-order plus delay system is added between the output of the controller and the input of the plant,

$$G(s) = \frac{1}{1 + 0.041\, s} e^{-0.0015\, s}.$$

In the global controller, we use the method presented in [31] to calculate ξ_e from $R_{0,e}$. Simulation results of this example are presented in Figs. 4–9. The results show that the end effector tracks the 6D pose trajectory well. From Figs. 7–8, it is seen that the position and attitude of the end effector can be tracked separately, which cannot be realized in a general quadrotor-based aerial manipulator. The two

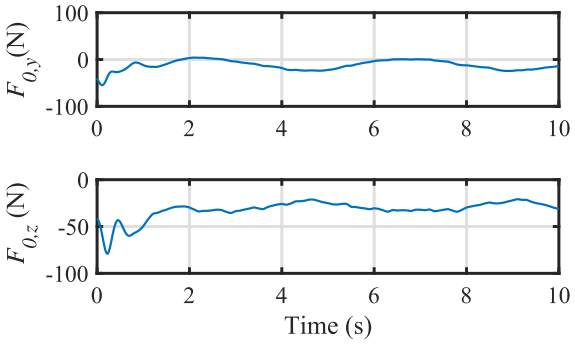

FIGURE 9. The force acting on the aircraft base.

elements of F_0 are shown in Fig. 9. In this example, $\langle F_0, e_3 \rangle$ is still the primary force, as there should exists force which is needed to compensate for the gravity. Because of big initial tracking error, $\langle F_0, e_2 \rangle$ is also big at initial stage. Figure 8 shows the evolution of the attitude error of the end effector. The attitude error is stabilized from biggest value. It is noted that because of the complex uncertainties, the attitude error is actually bounded, e.g., it converges to a small set containing origin but not zero. This numerical example demonstrates the theoretical analysis.

V. CONCLUSIONS

This paper has investigated the dynamics and control of a class of aerial manipulator for the purpose of 6D pose trajectory of the end effector. The differential flatness of the system has been analyzed. The conditions of the system with the proposed flat output have been obtained. It has been shown that it requires the aircraft platform to have a 2D actuation force. Although such a class of aircraft platform differs from the traditional under-actuated aerial vehicle. It is believed that the proposed kind of aircraft is still more efficient than the fully actuated aerial vehicle. A cascade structure controller has been designed. It has been proven that this controller archives independent 6D pose trajectory tracking for the end effector. It has also been shown that the proposed controller can stabilize all the states of the system, thus no unstable internal dynamics is induced. The proposed work provides a control framework for possible advanced tasks using aerial manipulators.

Future work can be conducted in several directions. First, real time implementation of the proposed aerial manipulator on a physical prototype is of interests. This will be a work in the area of mechatronics. Second, the trajectory planning and the force control using the proposed aerial manipulator can be further investigated.

REFERENCES

[1] X. Ding and Y. Yu, "Motion planning and stabilization control of a multipropeller multifunction aerial robot," *IEEE/ASME Trans. Mechatronics*, vol. 18, no. 2, pp. 645–656, Apr. 2013.
[2] N. Michael, D. Mellinger, Q. Lindsey, and V. Kumar, "The GRASP multiple micro-UAV testbed," *IEEE Robot. Autom. Mag.*, vol. 17, no. 3, pp. 56–65, Sep. 2010.

[3] V. Ghadiok, J. Goldin, and W. Ren, "Autonomous indoor aerial gripping using a quadrotor," in *Proc. IEEE/RSJ Int. Conf. Intell. Robots Syst.*, San Francisco, CA, USA, Sep. 2011, pp. 4645–4651.
[4] P. E. I. Pounds, D. R. Bersak, and A. M. Dollar, "Grasping from the air: Hovering capture and load stability," in *Proc. IEEE Int. Conf. Robot. Autom. (ICRA)*, Shanghai, China, May 2011, pp. 2491–2498.
[5] H. Lee and H. J. Kim, "Constraint-based cooperative control of multiple aerial manipulators for handling an unknown payload," *IEEE Trans. Ind. Informat.*, vol. 13, no. 6, pp. 2780–2790, Dec. 2017.
[6] S. Kim, H. Seo, J. Shin, and H. J. Kim, "Cooperative aerial manipulation using multirotors with multi-dof robotic arms," *IEEE/ASME Trans. Mechatronics*, vol. 23, no. 2, pp. 703–712, Apr. 2018.
[7] M. Orsag, C. Korpela, S. Bogdan, and P. Oh, "Dexterous aerial robots–mobile manipulation using unmanned aerial systems," *IEEE Trans. Robot.*, vol. 33, no. 6, pp. 1453–1466, Dec. 2017.
[8] M. Fumagalli, R. Naldi, A. Macchelli, R. Carloni, S. Stramigioli, and L. Marconi, "Modeling and control of a flying robot for contact inspection," in *Proc. IEEE/RSJ Int. Conf. Intell. Robots Syst.*, Vilamoura, Portugal, Oct. 2012, pp. 3532–3537.
[9] A. E. Jimenez-Cano, J. Martin, G. Heredia, A. Ollero, and R. Cano, "Control of an aerial robot with multi-link arm for assembly tasks," in *Proc. IEEE Int. Conf. Robot. Autom.*, May 2013, pp. 4916–4921.
[10] V. Lippiello *et al.*, "Hybrid visual servoing with hierarchical task composition for aerial manipulation," *IEEE Robot. Autom. Lett.*, vol. 1, no. 1, pp. 259–266, Jan. 2016.
[11] F. Huber *et al.*, "First analysis and experiments in aerial manipulation using fully actuated redundant robot arm," in *Proc. IEEE/RSJ Int. Conf. Intell. Robots Syst.*, Nov. 2013, pp. 3452–3457.
[12] M. Fumagalli *et al.*, "Developing an aerial manipulator prototype: Physical interaction with the environment," *IEEE Robot. Autom. Mag.*, vol. 21, no. 3, pp. 41–50, Sep. 2014.
[13] T. W. Danko, K. P. Chaney, and P. Y. Oh, "A parallel manipulator for mobile manipulating UAVs," in *Proc. IEEE Int. Conf. Technol. Practical Robot Appl. (TePRA)*, May 2015, pp. 1–6.
[14] H.-N. Nguyen, C. Ha, and D. Lee, "Mechanics, control and internal dynamics of quadrotor tool operation," *Automatica*, vol. 61, pp. 289–301, Nov. 2015.
[15] R. Naldi, P. Pounds, S. D. Marco, and L. Marconi, "Output tracking for quadrotor-based aerial manipulators," in *Proc. Amer. Control Conf. (ACC)*, Jul. 2015, pp. 1855–1860.
[16] B. Yüksel, G. Buondonno, and A. Franchi, "Differential flatness and control of protocentric aerial manipulators with any number of arms and mixed rigid-/elastic-joints," in *Proc. IEEE/RSJ Int. Conf. Intell. Robots Syst. (IROS)*, Oct. 2016, pp. 561–566.
[17] M. Tognon, B. Yüksel, G. Buondonno, and A. Franchi, "Dynamic decentralized control for protocentric aerial manipulators," in *Proc. IEEE Int. Conf. Robot. Autom. (ICRA)*, May 2017, pp. 6375–6380.
[18] Y. Yu, X. Ding, and J. J. Zhu, "Dynamic modeling and control for aerial arm-operating of a multi-propeller multifunction aerial robot," *Adv. Robot.*, vol. 31, no. 13, pp. 665–679, 2017.
[19] M. J. Kim, K. Kondak, and C. Ott, "A stabilizing controller for regulation of UAV with manipulator," *IEEE Robot. Autom. Lett.*, vol. 3, no. 3, pp. 1719–1726, Jul. 2018.
[20] H. Yang and D. Lee, "Dynamics and control of quadrotor with robotic manipulator," in *Proc. IEEE Int. Conf. Robot. Autom. (ICRA)*, Hong Kong, Jun. 2014, pp. 5544–5549.
[21] M. Ryll *et al.*, "6D physical interaction with a fully actuated aerial robot," in *Proc. IEEE Int. Conf. Robot. Autom. (ICRA)*, May 2017, pp. 5190–5195.
[22] M. Ryll, H. H. Bülthoff, and P. R. Giordano, "Modeling and control of a quadrotor UAV with tilting propellers," in *Proc. IEEE Int. Conf. Robot. Automat. (ICRA)*, May 2012, pp. 4606–4613.
[23] M. Tognon and A. Franchi, "Omnidirectional aerial vehicles with unidirectional thrusters: Theory, optimal design, and control," *IEEE Robot. Autom. Lett.*, vol. 3, no. 3, pp. 2277–2282, Jul. 2018.
[24] H. Romero, S. Salazar, and R. Lozano, "Real-time stabilization of an eight-rotor UAV using optical flow," *IEEE Trans. Robot.*, vol. 25, no. 4, pp. 809–817, Aug. 2009.
[25] T. Lee, "Geometric control of quadrotor UAVs transporting a cable-suspended rigid body," *IEEE Trans. Control Syst. Technol.*, vol. 26, no. 1, pp. 255–264, Jan. 2018.
[26] H.-N. Nguyen, S. Park, J. Park, and D. Lee, "A novel robotic platform for aerial manipulation using quadrotors as rotating thrust generators," *IEEE Trans. Robot.*, vol. 34, no. 2, pp. 353–369, Apr. 2018.
[27] D. Six, S. Briot, A. Chriette, and P. Martinet, "The kinematics, dynamics and control of a flying parallel robot with three quadrotors," *IEEE Robot. Autom. Lett.*, vol. 3, no. 1, pp. 559–566, Jan. 2018.
[28] S. K. Agrawal and V. Sangwan, "Differentially flat designs of underactuated open-chain planar robots," *IEEE Trans. Robot.*, vol. 24, no. 6, pp. 1445–1451, Dec. 2008.
[29] P. O. Pereira, R. Zanella, and D. V. Dimarogonas, "Decoupled design of controllers for aerial manipulation with quadrotors," in *Proc. IEEE/RSJ Int. Conf. Intell. Robots Syst. (IROS)*, Oct. 2016, pp. 4849–4855.
[30] J. S. Dai, "Euler–Rodrigues formula variations, quaternion conjugation and intrinsic connections," *Mechanism Mach. Theory*, vol. 92, pp. 144–152, Oct. 2015.
[31] Y. Yu and X. Ding, "A global tracking controller for underactuated aerial vehicles: Design, analysis, and experimental tests on quadrotor," *IEEE/ASME Trans. Mechatronics*, vol. 21, no. 5, pp. 2499–2511, Oct. 2016.
[32] A. R. Teel, F. Forni, and L. Zaccarian, "Lyapunov-based sufficient conditions for exponential stability in hybrid systems," *IEEE Trans. Autom. Control*, vol. 58, no. 6, pp. 1951–1956, Jun. 2013.
[33] H. K. Khalil, *Nonlinear Systems*. Upper Saddle River, NJ, USA: Prentice-Hall, 1991.
[34] S. Islam, P. X. Liu, and A. E. Saddik, "Robust control of four-rotor unmanned aerial vehicle with disturbance uncertainty," *IEEE Trans. Ind. Electron.*, vol. 62, no. 3, pp. 1563–1571, Mar. 2015.

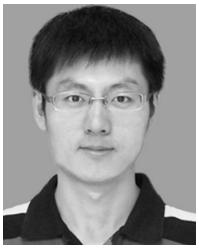

YUSHU YU received the B.S., M.S., and Ph.D. degrees in mechanical engineering from the Beijing University of Aeronautics and Astronautics (BUAA), Beijing, China, in 2007, 2010, and 2013, respectively. From 2013 to 2014, he was an Engineer with China Aerospace Science and Industry Corporation. He conducted research at the BUAA, Nanyang Technological University, Singapore, and the Chalmers University of Technology, Sweden, from 2014 to 2019. He is currently an Associate Professor with the Beijing Institute of Technology (BIT), China. His research interest includes control and robotics. He received the 2012 IEEE International Conference on Mechatronics and Automation Toshio Fukuda Best Award in Mechatronics, and the Excellent Doctoral Dissertation of BUAA, in 2014.

VINCENZO LIPPIELLO (SM'17) was born in Naples, Italy, in 1975. He received the Laurea degree in electronic engineering and the Research Ph.D. degree in information engineering from the University of Naples Federico II, Naples, in 2000 and 2004, respectively, where he is currently an Associate Professor of automatic control with the Department of Electrical Engineering and Information Technology. He has authored or coauthored more than 120 journal and conference papers and book chapters. His research interests include visual serving of robot manipulators, hybrid visual/force control, adaptive control, grasping and manipulation, aerial robotics, and visual object tracking and reconstruction.